

# Floquet Fractional Chern Insulator in Doped Graphene

Adolfo G. Grushin,<sup>1,2</sup> Álvaro Gómez-León,<sup>2</sup> and Titus Neupert<sup>3</sup>

<sup>1</sup>*Max-Planck-Institut für Physik komplexer Systeme, 01187 Dresden, Germany*

<sup>2</sup>*Instituto de Ciencia de Materiales de Madrid, CSIC, Cantoblanco, E-28049 Madrid, Spain*

<sup>3</sup>*Princeton Center for Theoretical Science, Princeton University, Princeton, New Jersey 08544, USA*

(Dated: February 22, 2022)

Fractional Chern insulators are theoretically predicted states of electronic matter with emergent topological order. They exhibit the same universal properties as the fractional quantum Hall effect, but dispose of the need to apply a strong magnetic field. However, despite intense theoretical work, an experimental realization for these exotic states of matter is still lacking. Here we show that doped graphene turns into a fractional Chern insulator, when irradiated with high-intensity circularly polarized light. We derive the effective steady state band structure of light-driven graphene using Floquet theory and subsequently study the interacting system with exact numerical diagonalization. The fractional Chern insulator state equivalent to the  $1/3$  Laughlin state appears at  $7/12$  total filling of the honeycomb lattice ( $1/6$  filling of the upper band). The state also features spontaneous ferromagnetism and is thus an example of the spontaneous breaking of a continuous symmetry along with a topological phase transition.

Fractional Chern insulators (FCIs) [1–5] have been discovered numerically in lattice models of two-dimensional electronic systems. They emerge as the ground state of repulsively interacting electrons that partially fill Bloch bands with a nontrivial topological attribute, namely a nonvanishing Chern number [6]. The time-reversal symmetry (TRS) breaking electronic hopping integrals on the lattice, that are responsible for the band topology, take the role played by the strong magnetic field in the fractional quantum Hall effect. FCIs show that fractional quantum Hall states can appear more generically than previously assumed, and do not rely on the specific energetical or analytical properties of Landau levels.

For a system to support a FCI ground state, the energetics have to satisfy specific conditions. For example, if the topological band is spectrally flat [1, 7, 8] or the energy scale of the repulsive interaction exceeds the energy scales of the band [9], FCIs are favored. This is why the experimental discovery of FCIs is still a formidable experimental challenge, despite the recent experimental realization of its “noninteracting” parent band structure, the Chern insulator or anomalous quantum Hall effect [10]. Needed are systems with a large amount of tunability, to meet both the topological and energetical requirements. Ultracold atomic gases in optical lattices [11], artificial graphene [12], photonic crystals [13], and light-driven solid state systems [14–16] are such tunable platforms, all of which have been shown to potentially host topological band structures.

In this study, we shall focus on light-driven graphene [see Fig. 1], for which several works have proved that circularly polarized light allows to open a gap in the Dirac cones, leading to a topologically nontrivial state, characterized by chiral edge states [15, 17, 18]. The resulting periodically driven steady state is theoretically described using Floquet theory and is thus called a Floquet Chern insulator. The key ingredients for its emergence are (i)

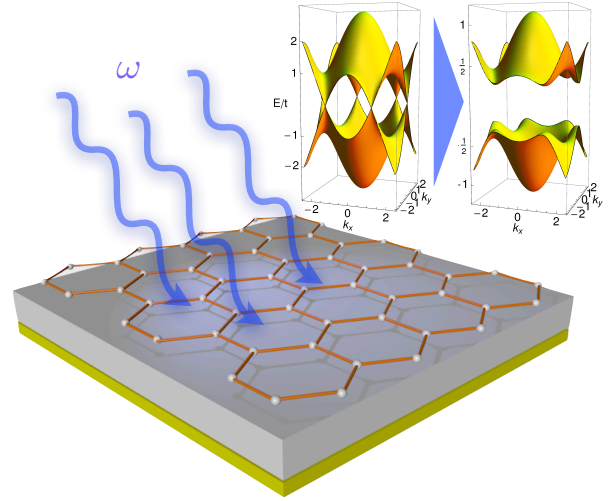


Figure 1: Sketch of the proposed experiment. A graphene-flake is irradiated with light of frequency  $\omega$  while a gate voltage is applied via a backgate (yellow) to change the band filling. In the high-frequency regime, the incident light changes the single-particle band structure into an effective Floquet band structure that acquired a gap at the Dirac points (shown are the Floquet bands for the electric field configuration  $A_x = A_y = 1.7$ ,  $\phi = \pi/2$ , and  $\omega = 10t_1$ ).

the critical nature of the Dirac electrons in graphene and (ii) the time-reversal symmetry breaking provided by the non-linearly polarized light [19].

Here, we show by means of numerical exact diagonalization that graphene at  $7/12$  total filling of the  $\pi$ -bands, when irradiated with high-intensity circularly polarized light, realizes a ferromagnetic FCI steady state, which we call a Floquet fractional Chern insulator (FFCI). The FFCI state is characterized by a three-fold topological groundstate degeneracy and a contribution to the Hall conductivity of  $\sigma_H = \frac{1}{3} \frac{e^2}{h}$ . Furthermore we prove

that the full  $SU(2)$  spin-rotation symmetry of the model Hamiltonian (the light-field does not couple to the spin and the spin-orbit coupling is negligible) is spontaneously broken for a ferromagnetic steady state, and gapless magnon excitations emerge, coexisting with the FFCI groundstate. We emphasize that we do not rely on a mean-field approximation to obtain this result [33].

*Floquet approach for ac driven graphene* We model irradiated monolayer graphene by considering spinful electrons that populate a honeycomb lattice  $\Lambda$  and interact repulsively via their on-site ( $U$ ) and nearest neighbor ( $V$ ) electronic densities  $n_{i,\sigma}$ , for  $i \in \Lambda$  and  $\sigma = \uparrow, \downarrow$ ,

$$H(\tau) := H_0(\tau) + H_{\text{int}},$$

$$H_{\text{int}} := U \sum_i n_{i,\uparrow} n_{i,\downarrow} + V \sum_{\langle i,j \rangle} \sum_{\sigma,\sigma'} n_{i,\sigma} n_{j,\sigma'}. \quad (1)$$

For the single particle Hamiltonian  $H_0(\tau)$ , we adopt the convention used in [1, 20]. The time dependence is induced via the electromagnetic vector potential  $\mathbf{A}(\tau, \phi) = (A_x \sin(\omega\tau), A_y \sin(\omega\tau + \phi), 0)^T$  of the external light field, where  $\omega$  is the frequency of the light,  $\phi$  is the phase difference,  $A_i = e\mathcal{E}_i a / \omega m_e$ ,  $e$  is the electron charge,  $m_e$  its mass,  $a$  the lattice spacing, and  $\mathcal{E}_i$  the  $i$ th component of the electric field. Only the single particle Hamiltonian  $H_0(\tau)$  is affected by this time dependence, and not the interaction Hamiltonian. The latter remains as in the undriven case since it is expressed in terms of the density operator.

Floquet theory provides a powerful formalism to study periodically driven systems. It allows to easily obtain effective time evolution operators, especially in the regime where the driving frequency is the dominant energy scale [21]. The single particle Hamiltonian, which enters the time dependent Schrödinger equation, can be obtained following Ref. [19] and the Supplementary Material, and has the Fourier decomposition

$$H_{0,\mathbf{k}}^q = \begin{pmatrix} 0 & (\rho_{\mathbf{k}}^{-q})^* \\ \rho_{\mathbf{k}}^q & 0 \end{pmatrix}, \quad \rho_{\mathbf{k}}^q = \sum_j t_{j,q}^F e^{i\mathbf{k} \cdot \mathbf{a}_j}, \quad (2)$$

where  $q \in \mathbb{Z}$  labels the Fourier component in frequency space, and the hopping integrals are given by  $t_{1,q}^F = t_1 J_q(A_y) e^{iq\phi}$ ,  $t_{2,q}^F = t_1 J_q(A_+) e^{iq\Psi_+}$ , and  $t_{3,q}^F = t_1 J_{-q}(A_-) e^{-iq\Psi_-}$ . Here,  $t_1$  is the nearest-neighbor hopping integral for electrons on the honeycomb lattice and  $J_q(A)$  denotes the Bessel functions of the first kind. The arguments of the Bessel functions contain the explicit electric field configuration  $A_{\pm} = \sqrt{\frac{3A_x^2}{4} + \frac{A_y^2}{4} \pm \frac{\sqrt{3}}{2} A_x A_y \cos(\phi)}$ , and the phase factors are given by  $\Psi_{\pm} = \arctan\left(\frac{A_y \sin(\phi)}{\sqrt{3}A_x \pm A_y \cos(\phi)}\right)$ . Finally, we define  $\mathbf{a}_1 = (0, 0)$ ,  $\mathbf{a}_2 = (\sqrt{3}, 3)/2$ , and  $\mathbf{a}_3 = (-\sqrt{3}, 3)/2$  as the unit cell vectors of the honeycomb lattice.

In this work we focus on the high frequency regime ( $\omega \gg t_1$ ), where the system dynamics can be accurately

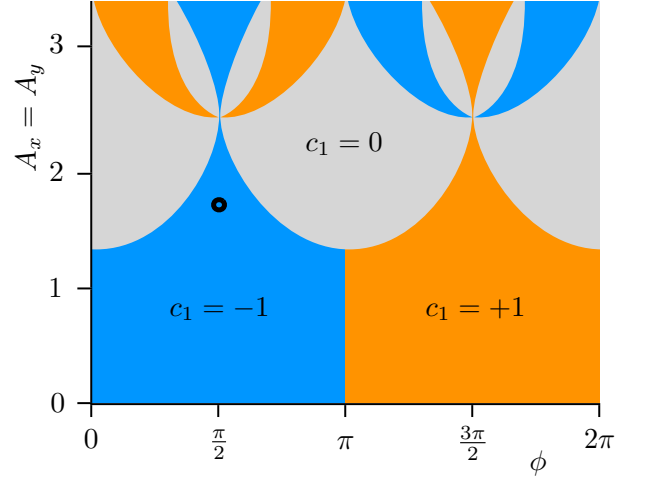


Figure 2: Topological phase diagram of periodically driven graphene at high frequency regime ( $\omega = 10t_1$ ) for circularly polarized light. The phase difference  $\phi$  and the field amplitude  $A_x = A_y$  allow to tune the Chern number of the lower spin-degenerate bands of the effective Floquet-Bloch Hamiltonian (3) between  $c_1 = -1$  and  $c_1 = +1$ . The black dot indicates the parameter values for which exact diagonalization calculations are presented in Figs. 3 and 4.

described by a static effective Hamiltonian, which can be expanded order by order in  $t_1/\omega$ . To zeroth order in  $t_1/\omega$ , the hopping integrals are renormalized by zeroth order Bessel functions only, with no breaking of TRS. To first order in  $t_1/\omega$ , corrections to the effective Hamiltonian must be considered due to hybridization with the nearest Floquet bands. Importantly, for non linear field polarization, TRS is broken by these corrections, a prerequisite to realize a Floquet Chern insulator. The effective Hamiltonian for long-time dynamics is then defined by including higher Fourier components of the Hamiltonian, leading to the  $2 \times 2$  Floquet-Bloch Hamiltonian (for details see the Supplementary Material):

$$H_{\text{eff},\mathbf{k}} = H_{0,\mathbf{k}}^0 - \frac{1}{\omega} \left( [H_{0,\mathbf{k}}^0, H_{0,\mathbf{k}}^{-1}] - [H_{0,\mathbf{k}}^0, H_{0,\mathbf{k}}^1] + [H_{0,\mathbf{k}}^{-1}, H_{0,\mathbf{k}}^1] \right). \quad (3)$$

Then, the effective single particle Hamiltonian expressed using the second-quantized operators  $c_{\mathbf{k},\sigma}^\dagger = (c_{\mathbf{k},\sigma,A}^\dagger, c_{\mathbf{k},\sigma,B}^\dagger)$ , that create an electron with momentum  $\mathbf{k}$  and spin  $\sigma$  in sublattice  $A$  and  $B$ , respectively, reads

$$H_{\text{eff},\mathbf{k}} := \sum_{\mathbf{k} \in \text{BZ}} \sum_{\sigma=\uparrow,\downarrow} c_{\mathbf{k},\sigma}^\dagger H_{\text{eff},\mathbf{k}} c_{\mathbf{k},\sigma}. \quad (4)$$

The Hamiltonian (4) has two pairs of spin-degenerate bands that touch in two Dirac points for  $t_1/\omega \rightarrow 0$ . The correction to first order in  $t_1/\omega$  in the  $2 \times 2$  Floquet-Bloch Hamiltonian  $H_{\text{eff},\mathbf{k}}$  is proportional to the third Pauli matrix  $\sigma_z$ . Due to the TRS breaking it can thus potentially

open a Haldane-type gap [6] in the spectrum, so that the resulting spin-degenerate bands can acquire a Chern number  $c_1 = \pm 1$  for each spin species. The phase diagram for different externally tunable parameters is shown in Fig. 2.

It is worth emphasizing that in the high frequency limit relevant for this work, the Hamiltonian (4) is a time independent effective Hamiltonian that governs stroboscopic evolution. Therefore, it allows to fill the bands as in the case of time independent systems.

*Exact diagonalization results* We are now going to show that the ground state of the Floquet Hamiltonian  $H_{\text{eff}} + H_{\text{int}}$ , and with this the steady state of the driven Hamiltonian (1), can be tuned into a FFCI by controlling (i) the filling of the system with electrons and (ii) the amplitude and phase of the light field. The emergence of a FFCI depends crucially on the ratios between the energy scales of the single-particle band gap  $\Delta$ , the single particle band width  $W$  and the repulsive electron-electron interactions, where mathematical band flatness is not always the optimal choice [22]. In graphene, the interaction parameters are given by  $U = 3t$  and  $V = 2t$  [23]. Choosing incident light with amplitude  $A_x = A_y = 1.7$  and the phase shift  $\phi = \pi/2$ , for example, results in an  $H_{\text{eff}}$  with  $\Delta/W = 0.6$ . We study the system above half-filling, so that the upper spin-degenerate band of  $H_{\text{eff}}$  is partially filled. Given the size of the single particle gap  $\Delta$ , it is reasonable to approximate the states in the lower band to be occupied with probability one, even in the interacting many-body ground state [9]. We thus ignore those single-particle states and project the degrees of freedom of the system to the upper spin-degenerate band of  $H_{\text{eff}}$  by means of the projector  $P$  and to study the Hamiltonian

$$H_{\text{proj}} = PH_{\text{eff}}P + PH_{\text{int}}P. \quad (5)$$

Previous studies have shown that FCI ground states equivalent to the  $1/m$  Laughlin state of the fractional Quantum Hall effect in Landau levels emerge quite generically if a flat band with Chern number  $c_1 = 1$  is populated with spineless fermions at a filling  $\nu = 1/m$ ,  $m \in \mathbb{Z}$  [1–3, 20]. In contrast, we are considering a *dispersionful* band with Chern number  $c_1 = 1$  that is partially filled with *spinful* electrons in such a way that the Hamiltonian is  $\text{SU}(2)$  spin-rotation symmetric. In anticipation of a spontaneous breaking of the  $\text{SU}(2)$  symmetry by the many-body ground state, we therefore study the system at  $\nu = 1/(2m)$  filling to obtain an FFCI that is equivalent to a  $\nu = 1/m$  Laughlin state. We have performed numerical exact diagonalization of the Hamiltonian (5) on lattices with  $L_x \times L_y = 4 \times 3$  and  $L_x \times L_y = 4 \times 6$  unit cells with  $N = 4$  and  $N = 8$  electrons, respectively, with periodic boundary conditions in place. Good quantum numbers of the many-body states are the total spin  $S = 0, \dots, N/2$ , the total spin- $z$  component

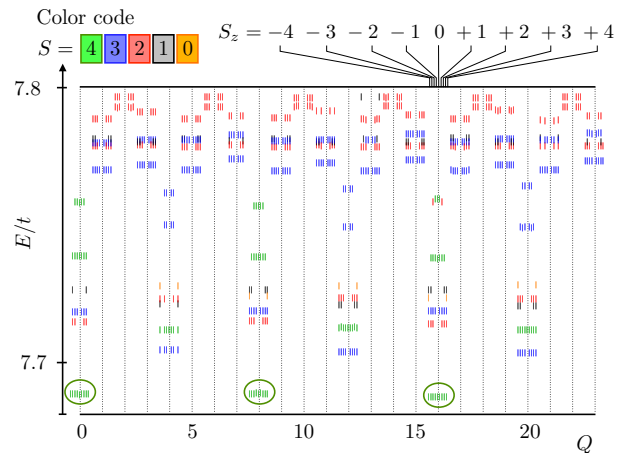


Figure 3: Low-lying portion of the energy spectrum of Hamiltonian (5) on a  $L_x \times L_y = 4 \times 6$  with  $N = 8$  particles. Encircled is the ground state manifold with 3-fold topological (quasi-) degeneracy of the fractional Chern insulator and  $N+1 = 9$  fold degeneracy as a precursor of spontaneous symmetry breaking toward a ferromagnetic phase in the thermodynamic limit. The good quantum numbers total momentum  $Q = k_x + L_x k_y$ , total spin  $S$  and total spin in  $z$  direction  $S_z$  are indicated.

$S_z = -N/2, \dots, N/2$  and the center of mass momentum  $Q \in [0, L_x \times L_y - 1]$ . All results and conclusions presented below extend to both lattice sizes and we focus on the  $L_x \times L_y = 4 \times 6$  lattice here, delegating the consistency check with  $L_x \times L_y = 4 \times 3$  to the Supplementary Material.

We observe that the low-energy states have both exact and approximate degeneracies: In each of the  $(N+1)$  sectors of  $S_z$ , three low-lying states are found which are not exactly, but approximately, degenerate. Each of these three states has an exactly degenerate partner in every other  $S_z$  sector (see Fig. 3). The total ground state degeneracy that we anticipate in the thermodynamic limit is thus  $3(N+1)$ . As all ground states have the maximum spin  $S = N/2$ , we interpret the exact  $(N+1)$ -fold degeneracy as a finite-size precursor of a spontaneous breaking of the  $\text{SU}(2)$  symmetry towards a ferromagnetic ground state in the thermodynamic limit. Both the tower-of-states structure [24] in the spectrum as a function of  $S$  [Fig. 4 (b)] and the exactness of the degeneracy support this conclusion (the order parameter  $S_z$  of ferromagnetism commutes with the Hamiltonian thus rendering the ground state degeneracy exact already for finite systems). In contrast, the 3-fold approximate degeneracy in each  $S_z$  sector is of topological origin. It is the  $m$ -fold topological ground state degeneracy of a  $1/m$  Laughlin state on the torus in the case  $m = 3$ . The non-local Wilson-loop order parameter does not commute with the Hamiltonian, rendering the degeneracy approximate in the finite system. Further supporting arguments that the three low-lying states in each  $S_z$  sector are indeed topo-

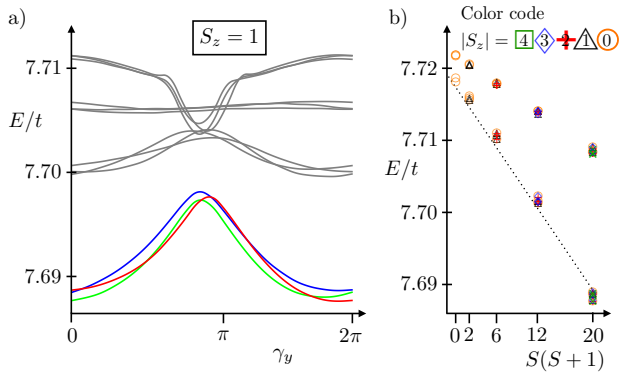


Figure 4: a) Spectral evolution of the energy spectrum of Fig. 3 in the sector with  $S_z = 1$  upon inserting a flux  $\gamma_y$  into the system, which is synonymous to twisting the boundary conditions in  $y$  direction with a complex phase  $e^{i\gamma_y}$ . The three fractional Chern insulator ground states evolve independently of the rest of the spectrum, and trade places, which signals their topological degeneracy and the charge fractionalization. b) The energy spectrum of Fig. 3 plotted against the total spin  $S(S+1)$  reveals the tower of states which evidencing the ferromagnetic nature of the ground state.

logically ordered FFCI states are: (i) By inserting a flux in the torus (which is equivalent to changing the boundary conditions from periodic to twisted [25]), the three states permute and return to their original order after three flux quanta [see Fig. 4 (a)]. This evidences charge fractionalization with quasiparticles of charge  $e/3$  and indicates that the topological groundstates survive in the thermodynamic limit. (ii) The three states occur at the momentum sectors  $Q$  that are predicted by the counting rule of Ref. [3] that is based on a  $1/3$  Laughlin state. (iii) Any superposition of the three ground states has a nearly constant charge density in position space, which excludes that these states would form a charge-density wave in the thermodynamic limit (see Supplementary Material).

From the presented results we conclude that the steady state of graphene at  $7/12$  total filling of the  $\pi$  bands (or  $1/6$  filling of the band above the Dirac cone) is a ferromagnetic FFCI. This distinct driven topological state has gapped charged excitations but supports gapless spin excitations, namely ferromagnetic magnons. The state features both conventional order and gapless topological order. Experimentally, its signature is a fractional contribution of  $\sigma_H = \frac{1}{3} \frac{e^2}{h}$  (in addition to the integer contribution of the lower band) defined for the driven system [26].

To certify the robustness of the FFCI state we have also tested its stability under changing some of the conditions discussed above. Firstly, we have investigated its fate upon changing to different light polarizations (using  $A_x/A_y = \sqrt{3}, 1/\sqrt{3}$  as two examples). The FFCI is still the groundstate of the system as long as the Chern number of the non interacting band is  $c_1 = \pm 1$ . Secondly, we

have investigated its appearance on a different lattice system. In particular, we find that for spinless electrons on the  $\pi$ -flux square lattice with nearest neighbor repulsive interaction the ground state is also the FFCI whenever  $(A_x = A_y, \phi)$  are such that the non-interacting bands have  $c_1 = \pm 1$  (see Supplementary Material). Both of these results evidence the ubiquitousness and robustness of the FFCI state.

*Experimental realization:* The practical realization of this novel state in graphene possess two experimental challenges. The first is to reach incident field amplitudes  $\mathcal{E}_x = \mathcal{E}_y \sim \omega \gg t_1$ . Although it is in principle possible to reach such a regime, today experiments have only explored amplitudes of one order of magnitude lower [27]. However, given the robustness and tuneability of the effect it is conceivable that lower frequencies and field amplitudes can in fact be sufficient to access the FFCI state in the thermodynamic limit. The second experimental issue is reaching the necessary filling factor of graphene's band structure. In particular, the electron density at  $1/6$  filling of the upper band is of the order of  $1 \times 10^{14} e/cm^2$ , still below the van Hove singularity in graphene. Even higher values up to the van Hove singularity have already been reached by chemical doping [28] and there are promising other routes by using for example polymer electrolytes [29]. Finally, other 2D materials with Dirac electrons such as silicene can potentially be used to tune the band structure parameters and host similar phases.

To summarize, we have found that doped graphene, irradiated with polarized light, undergoes an interaction driven spontaneous topological phase transition to a Floquet fractional Chern insulator (FFCI) state that features both topological and spontaneous ferromagnetic order. The robustness and tuneability of the FFCI state, appearing for different parameters, polarizations and lattices, evidences that this phase can be experimentally discovered in graphene. More generally, our work opens up a promising route to achieve tuneable realizations of elusive interacting fermionic and bosonic phases by periodically driving interacting systems.

*Acknowledgements:* We acknowledge E. Berg, D. Podolsky, G. Platero, M.A.H. Vozmediano, for useful discussions. Financial support from PIB2010BZ-00512 (A.G.G.), JAE program, MAT 2011-24331 and ITN, grant 234970 (EU) (A.G.-L.) and Swiss national science foundation (T.N.) is greatly acknowledged.

- 
- [1] T. Neupert, L. Santos, C. Chamon, and C. Mudry, Phys. Rev. Lett. **106**, 236804 (2011).
  - [2] D. Sheng, Z.-C. Gu, K. Sun, and L. Sheng, Nature Commun. **2**, 389 (2011).

- [3] N. Regnault and B. A. Bernevig, Phys. Rev. X **1**, 021014 (2011).
- [4] E. J. Bergholtz and Z. Liu, Int. J. Mod. Phys. B **27**, 1330017 (2013).
- [5] S. A. Parameswaran, R. Roy, and S. L. Sondhi (2013), arXiv:1302.6606.
- [6] F. D. M. Haldane, Phys. Rev. Lett. **61**, 2015 (1988).
- [7] E. Tang, J.-W. Mei, and X.-G. Wen, Phys. Rev. Lett. **106**, 236802 (2011).
- [8] K. Sun, Z.-C. Gu, H. Katsura, and S. Das Sarma, Physical Review Letters **106**, 236803 (2011).
- [9] S. Kourtis, J. W. Venderbos, and M. Daghofer, Phys. Rev. B **86**, 235118 (2012).
- [10] C.-Z. Chang, J. Zhang, X. Feng, J. Shen, Z. Zhang, M. Guo, K. Li, Y. Ou, P. Wei, L.-L. Wang, et al., Science **340**, 167 (2013).
- [11] T. Uehlinger, G. Jotzu, M. Messer, D. Greif, W. Hofstetter, U. Bissbort, and T. Esslinger, arXiv preprint arXiv:1308.4401 (2013).
- [12] K. K. Gomes, W. Mar, W. Ko, F. Guinea, and H. C. Manoharan, Nature **483**, 306 (2012).
- [13] M. C. Rechtsman, J. M. Zeuner, Y. Plotnik, Y. Lumer, D. Podolsky, F. Dreisow, S. Nolte, M. Segev, and A. Szameit, Nature **496**, 196 (2013).
- [14] N. H. Lindner, G. Refael, and V. Galitski, Nature Phys. **7**, 490 (2011).
- [15] T. Kitagawa, T. Oka, A. Brataas, L. Fu, and E. Demler, Phys. Rev. B **84**, 235108 (2011).
- [16] Á. Gómez-León, P. Delplace, and G. Platero, arXiv:1309.5402 (2013).
- [17] Z. Gu, H. A. Fertig, D. P. Arovas, and A. Auerbach, Phys. Rev. Lett. **107**, 216601 (2011).
- [18] T. Oka and H. Aoki, Phys. Rev. B **79**, 081406 (2009).
- [19] P. Delplace, Á. Gómez-León, and G. Platero, arXiv:1304.6272 (2013).
- [20] Y.-L. Wu, B. A. Bernevig, and N. Regnault, Phys. Rev. B **85**, 075116 (2012).
- [21] A. Gómez-León and G. Platero, Phys. Rev. Lett. **110**, 200403 (2013).
- [22] A. G. Grushin, T. Neupert, C. Chamon, and C. Mudry, Phys. Rev. B **86**, 205125 (2012).
- [23] T. Wehling, E. Şaşıoğlu, C. Friedrich, A. Lichtenstein, M. Katsnelson, and S. Blügel, Phys. Rev. Lett. **106**, 236805 (2011).
- [24] C. Lacroix, P. Mendels, and F. Mila, *Introduction to frustrated magnetism: Materials, experiments, theory*, vol. 164 (Springer, 2010).
- [25] Q. Niu, D. J. Thouless, and Y.-S. Wu, Phys. Rev. B **31**, 3372 (1985).
- [26] A. Kundu and B. Seradjeh, Phys. Rev. Lett. **111**, 136402 (2013).
- [27] S. Tani, F. Blanchard, and K. Tanaka, Phys. Rev. Lett. **109**, 166603 (2012).
- [28] J. L. McChesney, A. Bostwick, T. Ohta, T. Seyller, K. Horn, J. González, and E. Rotenberg, Phys. Rev. Lett. **104**, 136803 (2010).
- [29] A. Pachoud, M. Jaiswal, P. K. Ang, K. P. Loh, and B. Oezylmaz, Europhys. Lett. **92**, 27001 (2010).
- [30] J. Venderbos, S. Kourtis, J. van den Brink, and M. Daghofer, Phys. Rev. Lett. **108**, 126405 (2012).
- [31] X. G. Wen, F. Wilczek, and A. Zee, Phys. Rev. B **39**, 11413 (1989).
- [32] T. Neupert, L. Santos, C. Chamon, and C. Mudry, Phys. Rev. B **86**, 165133 (2012).
- [33] In previous work [30], a mean-field treatment was employed to obtain a magnetically ordered background and the resulting band structure was studied at partial filling, where the mean-field approximation is not justified anymore.

## Appendix A: Explicit calculation of the Floquet Hamiltonian

We initially consider the full time dependent Hamiltonian

$$H(\tau) = H_0(\tau) + U \sum_i n_{\uparrow,i} n_{\downarrow,i} + V \sum_{\langle i,j \rangle} \sum_{\sigma,\sigma'} n_{i,\sigma} n_{j,\sigma'}, \quad (\text{A1})$$

where

$$H_0(\tau) = \begin{pmatrix} 0 & \rho(\mathbf{k}, \tau)^* \\ \rho(\mathbf{k}, \tau) & 0 \end{pmatrix}, \quad \rho(\mathbf{k}, \tau) = \sum_{j=1}^3 t_j(\tau) e^{i\mathbf{k} \cdot \mathbf{a}_j},$$

and  $t_j(\tau) = t_1 e^{i\mathbf{A}(\tau) \cdot \mathbf{d}_j}$ , which is the usual coupling times a phase factor due to the presence of a vector potential. The vectors  $\mathbf{a}_j$  are the unit cell vectors  $\mathbf{a}_1 = a(0,0)$ ,  $\mathbf{a}_2 = (\sqrt{3}, 3)a/2$ ,  $\mathbf{a}_3 = (-\sqrt{3}, 3)a/2$ , and the distance to the nearest neighbors  $\mathbf{d}_j$  are given by  $\mathbf{d}_1 = a(0, -1)$ ,  $\mathbf{d}_2 = a(\sqrt{3}, 1)/2$ , and  $\mathbf{d}_3 = a(-\sqrt{3}, 1)/2$ . Importantly, the interaction terms does not couple to the ac field, which can be understood as follows: The interaction terms depend on the momentum difference between the electrons, and then for a spatially homogeneous fields this is time independent. Alternatively, as the coupling with the electric field can be also written as  $\vec{\mathcal{E}}(t) \cdot \vec{x}$ , where the electric field  $\vec{\mathcal{E}}(t) = -\partial_t \mathbf{A}(t)$ , the field will only couple to those terms which does not commute with the position operator. Therefore, on site interactions are proportional to the position operator and will not become time dependent.



Following Ref. [19] the Floquet operator can be calculated in Sambe space, leading to

$$\mathcal{H}_{0,\mathbf{k}}^q = \begin{pmatrix} 0 & (\rho_{\mathbf{k}}^{-q})^* \\ \rho_{\mathbf{k}}^q & 0 \end{pmatrix} - n\omega\delta_{n,m}, \quad \rho_{\mathbf{k}}^q = \sum_j t_{j,q}^F e^{i\mathbf{k}\cdot\mathbf{a}_j},$$

where the hoppings are

$$t_{1,q}^F = t_1 J_q(A_y) e^{iq\phi}, \quad t_{2,q}^F = t_1 J_q(A_+) e^{iq\Psi_+}, \quad \text{and} \quad t_{3,q}^F = t_1 J_{-q}(A_-) e^{-iq\Psi_-},$$

with  $q \equiv n - m$ , being  $n$  and  $m$  the Fourier components of the Fourier expansion of each Floquet state. The arguments of the Bessel functions and phase factors are

$$A_{\pm} = \sqrt{\frac{3A_x^2}{4} + \frac{A_y^2}{4} \pm \frac{\sqrt{3}}{2} A_x A_y \cos(\phi)}, \quad \Psi_{\pm} = \arctan\left(\frac{A_y \sin(\phi)}{\sqrt{3}A_x \pm A_y \cos(\phi)}\right).$$

To obtain the effective Hamiltonian let us consider a stroboscopic evolution operator over a period  $T$

$$U(T) = \mathcal{T} e^{-i \int_0^T H_0(\tau) d\tau} \simeq e^{-i H_{\text{eff}} T}.$$

Next, due to its time periodicity we consider the Fourier decomposition of the Hamiltonian

$$H_0(\tau) = \sum_{n=-\infty}^{\infty} H_0^n e^{in\omega\tau} \simeq H_0^0 + H_0^1 e^{i\omega\tau} + H_0^{-1} e^{-i\omega\tau}, \quad (\text{A2})$$

where we have considered just the first harmonic contribution, and  $H_0^{\pm 1} = \frac{1}{T} \int_0^T H_0(\tau) e^{\mp i\omega\tau} d\tau$ . Expanding the matrix exponential in Taylor series we obtain:

$$e^{-i \int_0^T H_0(\tau) d\tau} \simeq 1 - i \int_0^T H_0(\tau) d\tau + \frac{(-i)^2}{2} \int_0^T H_0(\tau_1) d\tau_1 \int_0^T H_0(\tau_2) d\tau_2 + \dots$$

Then, in terms of the previous expansion, the stroboscopic evolution operator is given by

$$\begin{aligned} U(T) &\simeq \mathcal{T} \left\{ 1 - i \int_0^T H_0(\tau) d\tau + \frac{(-i)^2}{2} \int_0^T H_0(\tau_1) d\tau_1 \int_0^T H_0(\tau_2) d\tau_2 \right\} \\ &= 1 - i \int_0^T H_0(\tau) d\tau - \frac{1}{2} \left[ \int_0^T d\tau_1 \int_0^{\tau_1} d\tau_2 H_0(\tau_1) H_0(\tau_2) + \int_0^T d\tau_2 \int_0^{\tau_2} d\tau_1 H_0(\tau_2) H_0(\tau_1) \right], \end{aligned}$$

where in the last line we have applied the time ordering operator  $\mathcal{T}$ . Using Eq. (A2) we can perform the time integrals, and reordering terms compare with the expansion of the effective time evolution operator

$$\begin{aligned} U(T) &\simeq 1 - i H_0^0 T - \frac{T}{\omega} \left\{ \pi (H_0^0)^2 - i ([H_0^0, H_0^{-1}] - [H_0^0, H_0^1] + [H_0^{-1}, H_0^1]) \right\} \\ &\simeq 1 - i H_{\text{eff}} T - \frac{1}{2} H_{\text{eff}}^2 T^2 + \dots \end{aligned}$$

The effective Hamiltonian is finally given by

$$H_{\text{eff}} = H_0^0 - \frac{1}{\omega} ([H_0^0, H_0^{-1}] - [H_0^0, H_0^1] + [H_0^{-1}, H_0^1]), \quad (\text{A3})$$

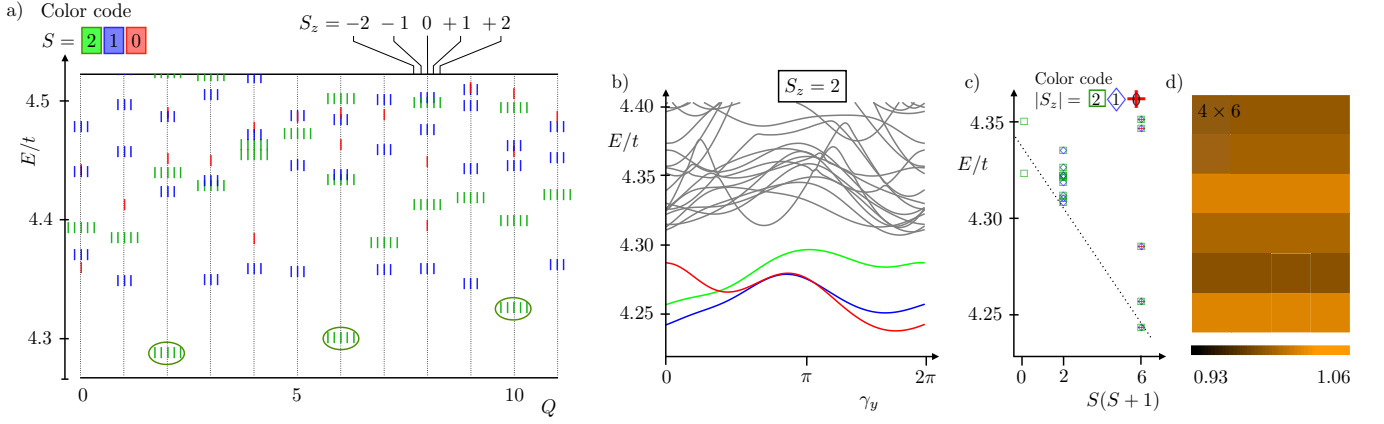


Figure 5: a) Many-body spectrum, b) flux insertion, and c) tower-of-states for the same parameters for a  $L = 4 \times 3$  lattice that evidence the presence of a ferromagnetically ordered FFCI state. d) We show also the local density profile  $n_r^{(i)}$  for the case of a  $L = 4 \times 6$  lattice defined in (B2) for one representative many-body groundstate. The small density variation is symptomatic of the FCI state.

which is eq. (3) of the main text. Explicitly, the single particle Hamiltonian in  $\mathbf{k}$  domain  $H_{\text{eff},\mathbf{k}} = t_1 \vec{g}(\mathbf{k}) \cdot \vec{\sigma}$  is given by

$$\begin{aligned}
 g_x &= -J_0(A_-) \cos\left(\frac{\sqrt{3}}{2}k_x - \frac{3}{2}k_y\right) + J_0(A_+) \cos\left(\frac{\sqrt{3}}{2}k_x + \frac{3}{2}k_y\right) + J_0(A_y), \\
 g_y &= J_0(A_-) \sin\left(\frac{\sqrt{3}}{2}k_x - \frac{3}{2}k_y\right) - J_0(A_+) \sin\left(\frac{\sqrt{3}}{2}k_x + \frac{3}{2}k_y\right), \\
 g_z &= -\frac{4t_1}{\omega} \left\{ J_0(A_+) \left[ J_1(A_-) \cos(\sqrt{3}k_x) \cos(\Psi_-) - J_1(A_+) \cos(\Psi_+) + J_1(A_y) \cos(\phi) \cos\left(\frac{\sqrt{3}}{2}k_x + \frac{3}{2}k_y\right) \right] \right. \\
 &\quad + J_0(A_-) \left[ J_1(A_-) \cos(\Psi_-) - J_1(A_+) \cos(\sqrt{3}k_x) \cos(\Psi_+) + J_1(A_y) \cos(\phi) \cos\left(\frac{\sqrt{3}}{2}k_x - \frac{3}{2}k_y\right) \right] \\
 &\quad + J_0(A_y) \left[ J_1(A_-) \cos(\Psi_-) \cos\left(\frac{\sqrt{3}}{2}k_x - \frac{3}{2}k_y\right) - J_1(A_+) \cos(\Psi_+) \cos\left(\frac{\sqrt{3}}{2}k_x + \frac{3}{2}k_y\right) + J_1(A_y) \cos(\phi) \right] \\
 &\quad - J_1(A_y) \left[ J_1(A_-) \sin\left(\frac{\sqrt{3}}{2}k_x - \frac{3}{2}k_y\right) \sin(\Psi_- + \phi) + J_1(A_+) \sin\left(\frac{\sqrt{3}}{2}k_x + \frac{3}{2}k_y\right) \sin(\phi - \Psi_+) \right] \\
 &\quad \left. + J_1(A_-) J_1(A_+) \sin(\sqrt{3}k_x) \sin(\Psi_- + \Psi_+) \right\}.
 \end{aligned}$$

Eq. (A3) is the single particle Hamiltonian considered all throughout this work. From it it is possible to extract a topological phase diagram for the Chern number  $c_1$  as a function of the external parameters of the electric field shown in Fig. 2. The band structure for the point  $A_x = A_y = 1.7$ , and  $\phi = \pi/2$  focus of this work is shown in Fig. 1.

## Appendix B: Further numerical evidence in favor of the presence and robustness of the Floquet fractional Chern insulator phase:

In this section, additional numerical results mentioned in the main text are presented as supporting evidence for the ferromagnetic Floquet fractional Chern insulator (FFCI).

### 1. Spectrum and Tower of states for $L = 4 \times 3$ $N = 4$

First, we focus on a different lattice size,  $L = 4 \times 3$  with  $N = 4$  particles, to compare with  $L = 4 \times 6$  with  $N = 8$  particles discussed in the main text. The spectrum, flux insertion and tower-of-states for this lattice size is presented in Fig. 5 (a)-(c). The figures show the same qualitative features as for the  $L = 4 \times 6$  lattice case discussed in the main text.

Firstly, as shown in Fig. 5 (a) the groundstate is three-fold degenerate for each  $S_z$  sector. The groundstates appear at the total momenta  $Q$  predicted by the counting rule of Ref. [3]. Under an adiabatic flux insertion in the  $\gamma_y$  direction, the states interchange signalling the topological degeneracy and charge fractionalization [see Fig. 5 (b)]. Furthermore, all groundstates have the maximum spin  $S = N/2$  which is evidence for the ferromagnetic nature of the FFCI state. This picture is further supported by the tower-of-states of Fig. 5 (c) that shows that the higher values of  $S(S+1)$  have the lowest energy, a finite size signature of the thermodynamic spontaneous symmetry breaking of the  $SU(2)$  symmetry, as discussed in the main text.

### 2. Charge density profile:

To ascertain the topological nature of the Floquet fractional Chern insulator state it is important to rule out the possibility of the appearance of a charge density wave (CDW) order, since both states can present the same momentum counting [20]. A way to distinguish between both phases was put forward in Ref. [22] by calculating the real space density profile, a procedure that we follow here. To this extent, we consider the local density operator defined by

$$\rho_{\mathbf{r}} := \frac{1}{L_1 L_2} \sum_{\mathbf{q}, \mathbf{k}} \sum_s e^{i \mathbf{q} \cdot \mathbf{r}} c_{\mathbf{k}+\mathbf{q}, s}^\dagger c_{\mathbf{k}, s}, \quad (\text{B1a})$$

For the quasi degenerate ground state manifold  $|\Psi_1\rangle, \dots, |\Psi_n\rangle$  ( $n = 3$  for the Laughlin state) we construct the matrix with elements

$$\varrho_{\mathbf{r}; ij} := \langle \Psi_i | \rho_{\mathbf{r}} | \Psi_j \rangle. \quad (\text{B1b})$$

The next step is to obtain a set of  $n$  maps of the local fermion density in the ground-state manifold. Labelling  $v_{\rho; \mathbf{r}_0}^{(i)}$ ,  $i = 1, \dots, n$  the set of orthonormal eigenvectors of  $\varrho_{\mathbf{r}_0}$  at some arbitrarily chosen site  $\mathbf{r}_0$  we evaluate the  $n$  real functions

$$n_{\mathbf{r}}^{(i)} := v_{\rho; \mathbf{r}_0}^{(i)\dagger} \varrho_{\mathbf{r}} v_{\rho; \mathbf{r}_0}^{(i)}, \quad i = 1, \dots, n. \quad (\text{B2})$$

The functions  $n_{\mathbf{r}}^{(i)}$  are density maps that show the variation of the local fermion density in position space. Featureless or flat density maps would be strong evidence in favour of an FCI. Therefore, finding strongly patterned density maps is a signature of a ground-state manifold that supports a CDW.

A typical charge density map for the three-fold ground state manifold of the FFCI state is shown in Fig. 5(d) for the particular point  $A_x = A_y = 1.7$   $\phi = \pi/2$  discussed in the main text. The density variation in position space is small, of about  $\sim 5\%$  which is indication of a FCI state. We attribute the small deviation to the lattice anisotropy, already observed in Ref. [22].

### 3. FFCI for different polarizations and lattices:

The FFCI state described in the main text appears for circular polarization  $A_x = A_y$ . Although we have focused on  $A_x = A_y = 1.7$ , a similar behaviour is observed in the vicinity of such point. In this section we show that the appearance of the FFCI state with this particular polarization (circular) and for the honeycomb lattice is not a fine tuned unique situation.

*Elliptical polarization:* We observe that this state also appears for elliptical polarization. In Fig. 7 (b) we show the phase diagram for the case where  $A_x/A_y = \sqrt{3}$  on the  $(A_x, \phi)$  phase space. As in the circular polarization, there are regions in the phase diagram where the effective bands have a non trivial Chern number  $c_1 = 1$ . For concreteness we consider the  $S_z = 0$  sector and  $A_x/A_y = \sqrt{3}$  with  $A_y = 0.9$ ,  $\phi = \pi/2$  for a  $L = 6 \times 4$  lattice with  $N = 8$  particles



taking  $\omega = 10t$ , without single particle dispersion (unlike in the main text). We note that adding dispersion only constrains the region of the phase diagram where the FFCI phase appears but does not eliminate it from the phase diagram. As in the main text, we compute the many-body spectrum via exact-diagonalization. The results are shown in Fig. 6 where (a) shows the many body energy spectrum (b) the flux insertion and (c) a representative local density profile.

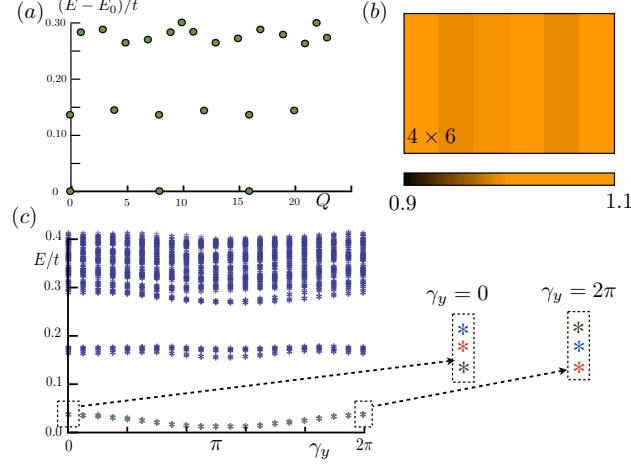


Figure 6: (a) The energy spectrum for the driven honeycomb lattice model with  $A_x/A_y = \sqrt{3}$  and  $A_y = 0.9$ ,  $\phi = \pi/2$  for a  $L = 6 \times 4$  lattice with  $N = 8$  particles against the total momentum  $Q$ . The three FCI states appear at momenta predicted by the counting rule of Ref. [3] (b) Density profile  $n_r^{(i)}$  defined in (B2) for one representative many-body groundstate. (c) Spectral evolution of the energy spectrum of (a) in the sector upon inserting a flux  $\gamma_y$  into the system. The zoom shows the interchange of the three fractional Chern insulator groundstates under one flux period and thus their topological degeneracy and charge fractionalization.

All three figures point to the realization of the FCI state since the ground state fall at the total momentum sectors  $Q$  expected from the counting rule of Ref. [3], they mix and interchange with each other under adiabatic flux insertion and the density profile is relatively uniform, as discussed in the previous section and in the main text. We nevertheless note that the relative density change is close to 10%, approximately twice the value for the circular polarization. We have also checked that all these three features also appear for different elliptical polarization such as  $A_x/A_y = 1/\sqrt{3}$ .

*$\pi$ -flux lattice:* The above results strongly indicate that the FFCI state described in the main text does not depend strongly on light polarization but rather on that the Chern number is finite. We have also studied whether this still holds for different lattices and find that indeed the honeycomb lattice is not a fine-tuned case. To support this claim we hereby provide numerical evidence of the appearance of the same  $1/3$  FFCI state for the  $\pi$ -flux lattice at half-filling. Because of the historical relevance of the model in condensed matter these results are interesting on their own right and therefore here we will sum up the most relevant results and further detail will be presented elsewhere.

Following the procedure outlined in the first section of this supplementary material, we have calculated the effective Hamiltonian  $H_{\text{eff}}$  corresponding to the  $\pi$ -flux model [31] with the conventions of Ref. [1]. The non-interacting phase diagram for this case, analogous to Fig. 2 in the main text for the honeycomb lattice is shown in Fig. 7 (a). As in the honeycomb case, there are regions in the parameter space  $(A_x = A_y, \phi)$  where the Chern number of the effective bands is non-trivial and takes the values  $c_1 = \pm 1$ .

Again, we consider only the fully polarized spin sector  $S_z = 0$  with a  $L = 6 \times 4$  lattice with  $N = 8$  particles and include band dispersion and  $\omega = 10t$ . Choosing the particular point  $A_x = A_y = 1.5$  and  $\phi = 1.65$  corresponding to the non-trivial case with  $c_1 = 1$  we find a three fold degenerate ground state as shown in the spectrum of Fig. 8 (a) together with the flux insertion in (b) and a representative local density profile (c). All three figures point to the realization of the FCI state: (i) the momentum sectors for the groundstate manifold coincide with those predicted by the counting rule of Ref. [3], (ii) the flux insertion reveals that the groundstates evolve independently and interchange upon one flux insertion and (iii) the uniformity of the density profile discards the CDW state as the many body ground state. Therefore, we conclude that the Floquet fractional Chern insulator state is also realized in the  $\pi$ -flux

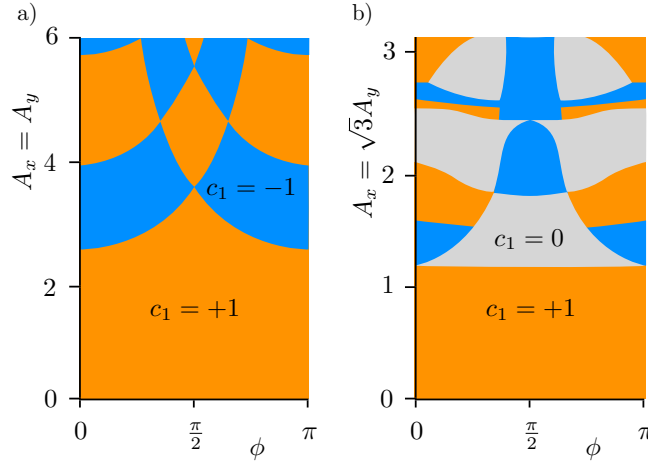


Figure 7: Chern number phase diagram for a) the square lattice Hamiltonian circularly polarized light and b) graphene with elliptically polarized light.

lattice. Furthermore, the symmetries of the square lattice make the sampling of the berry curvature BZ particularly uniform favouring the use of the simple formula of Ref. [32]. With this we have checked that the Hall conductivity of this system is closely quantized to  $\sigma_H \simeq \frac{1}{3} \frac{e^2}{h}$  as expected for the FCI state. We found that for this lattice the FCI state is defined in an even wider region of the phase diagram as compared to the honeycomb case details of which will be reported elsewhere.

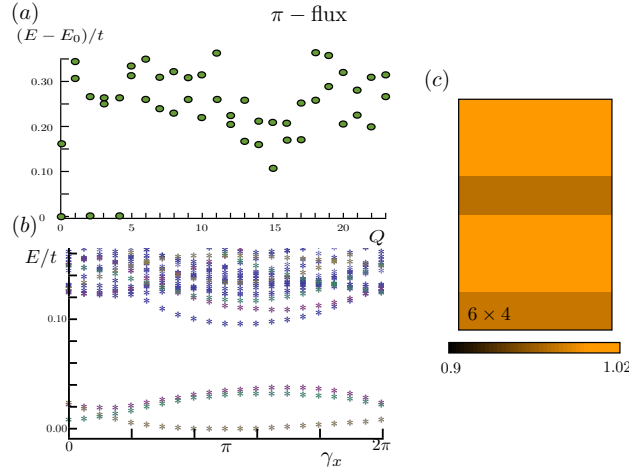


Figure 8: Floquet fractional Chern insulator state for the  $\pi$ -flux model with  $A_x = A_y = 1.6, \phi = 1.65, S_z = 0$  and  $L = 6 \times 4, N = 8$ . (a) The energy spectrum for the  $\pi$ -flux model against the total momentum  $Q$ . The three FCI states appear at momenta predicted by the counting rule of Ref. [3] (b) Spectral evolution of the energy spectrum of (a) in the sector upon inserting a flux  $\gamma_x$  into the system. The evolution of the three fractional Chern insulator ground states signals their topological degeneracy and charge fractionalization. c) Density profile  $n_r^{(i)}$  defined in (B2) for one representative many-body groundstate.